

High-temperature domain wall current in Mg-doped lithium niobate single crystals up to 400°C

Uliana Yakhnevych,¹ Marlo Kunzner,¹ Leonard M. Verhoff,² Julius Ratzenberger³,⁴ Elke Beyreuther³,⁵ Michael Rüsing⁴,⁶ Simone Sanna²,⁵ Lukas M. Eng³,⁵ and Holger Fritze^{1,6}

¹*Institut für Energieforschung und Physikalische Technologien, Technische Universität Clausthal, Am Stollen 19B, 38640 Goslar, Germany*

²*Institut für Theoretische Physik and Center for Materials Research (ZfM/LaMa), Justus-Liebig-Universität Gießen, Heinrich-Buff-Ring 16, 35392 Gießen, Germany*

³*Institut für Angewandte Physik, Technische Universität Dresden, Nöthnitzer Straße 61, 01187 Dresden, Germany*

⁴*Integrated Quantum Optics, Institute for Photonic Quantum Systems (PhOQS), Paderborn University, 33098 Paderborn, Germany*

⁵*Dresden-Würzburg Cluster of Excellence - EXC 2147, Technische Universität Dresden, 01062 Dresden, Germany*

⁶*Forschungszentrum Energiespeichertechnologien, Technische Universität Clausthal, Am Stollen 19A, 38640 Goslar, Germany*

(*Electronic mail: uliana.yakhnevych@tu-clausthal.de)

(Dated: 2 April 2024)

Conductive ferroelectric domain walls (DWs) represent a promising topical system for the development of nanoelectronic components and devices. DWs may show very different properties as compared to their bulk counterparts. Of central interest here is the domain wall current (DWC) of charged DWs in 5mol% Mg-doped lithium niobate single crystals; in contrast to former works, we extend the DWC study here to temperatures as high as 400°C. Both the temporal stability and the thermal activation energies of 100 - 160 meV are readily deduced from current-voltage sweeps as recorded over multiple heating cycles. Our experimental work is backed up by atomistic modelling of the DWC. The latter suggests that a large band bending renders head-to-head (H2H) and tail-to-tail (T2T) DWs semimetallic. These detailed investigations underline the potential to extending DWC-based nanoelectronic applications even into the so-far unexplored high-temperature regime.

Single-crystalline lithium niobate (LN) is the *drosophila* ferroelectric for applications based on piezoelectricity, electro-optical effects, or polarization switching. Devices include precision actuators, non-volatile ferroelectric random-access memories, electro-optical modulators, photovoltaic cells, resistive switches, and sensors for measuring vibration and magnetic fields, even at higher temperatures^{1,2}.

One major key factor that contributes to the versatility of LN-based devices is the ability to elegantly engineer ferroelectric domains and domain walls (DWs) into these crystals²⁻⁶. Domain engineering in LN involves the controlled creation and manipulation of DWs⁷. Recently, considerable advancements have been reported for fabricating and tuning the DW properties in LN crystals, specifically also to reproducibly increase the DW conductivity (DWC) by several orders of magnitude^{5,8-10}, which is of clue interest to the work here. Controlling the DWC has a broad impact for various devices, such as resistive switches, diode structures, or neuromorphic computing¹¹⁻¹⁴. For sensing devices, the ability to manipulate the DWC in LN offers promising prospects, provided they meet the challenging environmental conditions of i.e. high temperatures, as requested for instance in aerospace and automotive applications¹⁵. In fact, despite some minor hints towards a thermally-activated DWC process up to 70°C, studies on this topic have only rarely been reported^{8,16} and the high

temperature behavior and stability of domains and DWs remains unclear to date. While domains in LN endure annealing up to the Curie temperature T_c at 1100°C, the stability and enhanced conductivity of DWs is uncertain due to their non-equilibrium, inclined structure⁹.

By today, the electrical transport mechanism along charged ferroelectric DWs in LN (and also in many other ferroelectrics) is understood partly, only^{4,16-18}. While the formation of a 2-dimensional electron gas (2DEG) at strongly charged walls is proposed and experimentally investigated by many works¹⁸⁻²⁰, DWC measurements also support a thermally-activated process at less-inclined and less-charged DWs, e.g., in LN¹⁶. This contradicts the metallic-nature of a 2DEG, where no signatures of thermal activation should appear. Hence, two different DWC models result:

- The band-bending concept below the Fermi-level due to strong electric field discontinuities at inclined and charged DWs, leading to the formation of a 2DEG^{18,19};
- The defect-mediated hopping process of (mobile) screening charges along charged DWs, e.g. bound to polaron levels^{17,21}.

To clarify these issues, we (i) investigate the DWC in LN at elevated temperatures up to 400°C. This allows to proving the

existence of thermally-activated processes beyond room temperature, and hence to discriminating between the two mechanisms proposed above. Furthermore, (ii) we present DFT-calculated band structures of fully charged DWs in LN, in order to support whether or not the 2DEG theory accounts also for the DWC as observed here in LN-DWs.

In our experiments, z-cut 5mol% Mg-doped LN wafers from Yamaju Ceramics Co., Ltd., are used for domain engineering. Every sample piece measures 200 μm in thickness, and has a lateral size of 5 mm \times 6 mm. Single, hexagonally-shaped domains of a 110 - 300 μm diameter are fabricated by means of our UV-assisted electric field poling technique^{9,22}. In total, we investigated three different samples in this study, tagged as LN1, LN2, and LN3. Note that sample LN1 carries one such poled domain only, while two broadly separated domains *a* and *b* were poled into samples LN2 and LN3; LN2-*a* and LN2-*b* hence refer to the domain *a* and *b* in sample LN2, respectively. This variation aims at exploring potential relationships between domain size, current flow, and thermal stability. Domain formation is monitored *in-situ* via polarized light microscopy. Individual domains are then electrically contacted by depositing a 10-nm-thick Cr-electrode via magnetron sputtering onto both z-facets, and wired up to our electrical measuring units through conductive silver-paste contacts. As-grown DWs typically have a very low conductivity at room temperature (RT) that then is enhanced by several orders of magnitude following the protocol of Godau et al.^{5,9}.

DWC investigations in the temperature range of 25-400°C are then carried out by mounting the sample onto a ceramic heating element. Current-voltage (I-V) sweeps between ± 10 V are recorded using a Keithley 6517B electrometer connected to a μ -impedance setup, applying voltage increments of 1.48 V and a waiting time per step of 10 seconds. Using the μ -impedance setup bears two advantages, firstly in allocating individual DWs and surface spots with high precision through x-y positioning the top-contact platinum tip, while secondly, facilitating data acquisition at various temperatures considering a heating rate of 1 K/min, only.

Fig. 1 displays the typical DWC I-V characteristics for sample LN3-a at different stages and temperatures. Directly after domain poling illustrated also by the polarized microscopy image (see inset in Fig. 1a) the DWC at RT is negligibly small across the full ± 10 V range (black curve in Fig. 1a), while showing a drastic increase of up to six orders of magnitude after enhancement (red curve in Fig. 1a). Note that all DWs studied in this work exhibit an ohmic behavior after enhancement, while in previous works often rectifying characteristics have been reported as well^{5,9,16}. We find absolute room temperature DWCs ranging from $\sim 10^{-7}$ to $\sim 10^{-6}$ A at a +9 V bias voltage for all DWC measurements in all three samples, with differences being indicative for their effective and averaged DW inclination angle with respect to the sample c-axes⁹. Notably, the DWCs studied here show no dependence on either the DW area or size.

Fig. 1b presents the DWC I-V-curves recorded from DW LN3-a at elevated temperatures, i.e. at 100 °C (green), 350 °C

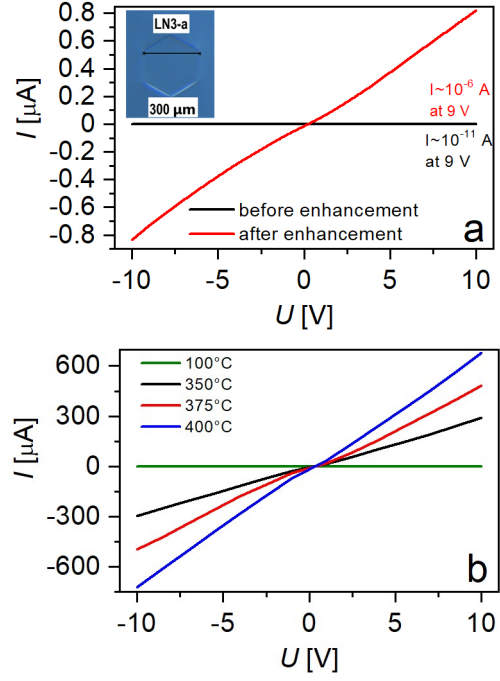


FIG. 1: I-V-characteristic across the ± 10 V voltage bias regime of the domain wall current (DWC) in sample LN3-a. (a) DWC before (black) and after (red) conductivity enhancement at room temperature; and (b) DWC recorded at elevated temperatures up to 400°C. Note the ohmic behavior of all I-V-curves, being independent on temperature or domain size. The inset in (a) depicts the DW contour of sample LN3-a, as recorded by polarized light microscopy.

(black), 375 °C (red), and 400 °C (blue). Notably all I-V-curves behave ohmic-like, while the DWC at 400 °C is increased at least $600 \times$ as compared to the RT DWC.

Fig. 2 displays the DWC recorded at a +7 V bias voltage for samples LN1-a and LN3-a in the Arrhenius-type plot, together with the DWC data from a bulk LN reference sample containing no DW at all (plotted in orange). The DWC increases as a function of rising temperatures for all samples, including the bulk reference. This trend is observed consistently either for increasing or decreasing temperature sweeps. Of particular interest is the comparison between investigated DWCs and bulk LN currents, as depicted in Fig. 2. The bulk LN current follows from conductivity data obtained through impedance spectroscopy^{23,24}; here, currents were calculated based on the sample thickness and average electrode size. Note the huge increase in the current magnitude between the bulk reference and samples LN1-a and LN3-a, respectively, displaying a six-order-of-magnitude difference at 250 °C. Therefore, we can exclude any bulk related contribution to the measured DWCs.

Moreover, we notice in Fig. 2 temperature ranges (marked with solid lines and annotated in Roman numerals: I, II, III) that show a linear increase in DWC, however, with different slopes, indicating thermally activated transport processes with different activation energies. We see from Fig. 2 that different

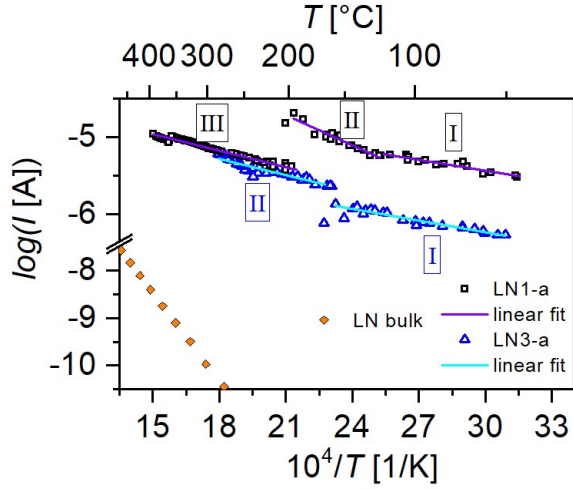


FIG. 2: Temperature-dependent DWC plotted for DW-sample LN1-a (purple) and LN3-a (blue) at a +7 V bias voltage. For reference, the bulk LN current (in orange) is displayed in the same Arrhenius plot.

DWC samples (here LN1-a and LN3-a) scatter by one order of magnitude in the absolutely measured DWC (see the DWC data for sample LN1-a and LN3-a at RT in Fig. 2). This trend persists up to approximately 200°C, hence branding the region I in Fig. 2. Above that threshold of 200°C, DWC data scatter less, (region II) and the differences gradually diminish, converging practically to the same DWC value for all analyzed DWs (in region III). These findings suggest that the DW morphology plays no major role anymore above the 200°C threshold.

Fig. 3 presents the activation energy E_A for all investigated DWCs as extracted by fitting $I \sim \exp(E_A/k_B T)$ to the linear segments I, II, and III in Fig. 2. The temperature intervals used for data fitting are the same ones as the ones delineated in Fig. 2. In addition, Fig. 3 contains also the as-deduced E_A for DW LN2-a, depicted for both its initial DWC state (solid black line) and the subsequent heating cycles 1 (green solid line) and 2 (green dashed line). Remarkably, our findings suggest that the studied domains maintain stable during repeated heating cycles. This implies a promising potential for utilizing DWC-based devices at elevated temperatures.

Our observations in Fig. 3 reveal two distinct activation energy levels, measuring approximately $E_A = 100$ meV and 160 meV. The data analysis delineates the temperature ranging into two overlapping regimes: room to medium temperatures (25 - 280°C) and temperatures above about 150°C. Werner et al.⁸ and Zahn et al.¹⁶ reported E_A values of 100 meV and 200 meV for the temperature range from -193°C to 70°C. They also suggested that the dominant charge carrier type for DWC in these DWs is of electronic nature, backed up by both recent Hall-transport measurements¹⁷ and strain vs. conductivity investigations²⁵, specifically involving thermally activated electron-polaron hopping. We assume that the activation energy values obtained here, ranging from 90 meV to 160 meV,

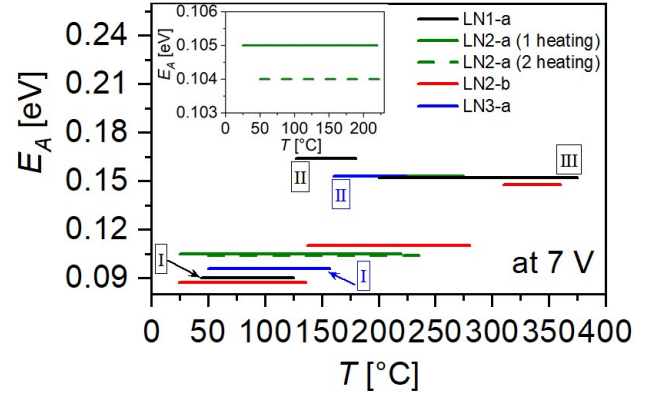


FIG. 3: Activation energies E_A of the DWC for the distinct temperature ranges as marked in Fig. 2. Note the reproducible E_A values of DW LN2-a even after several heating cycles.

also indicate involvement of electron-polaron hopping processes; in fact, such E_A values align well with the reported values for electron-polaron jumps in bulk lithium niobate^{26–28}.

It is evident from our experiments that DWs exhibit distinct activation energies across different temperature ranges. This implies the involvement of more than one type of defect/polaron that contributes to the DWC. Significantly, the presence of varied activation energies at both room and high temperatures consistently observed within the same sample, suggests that these differences are not sample-specific but likely associated with the DW morphology, which will require further studies.

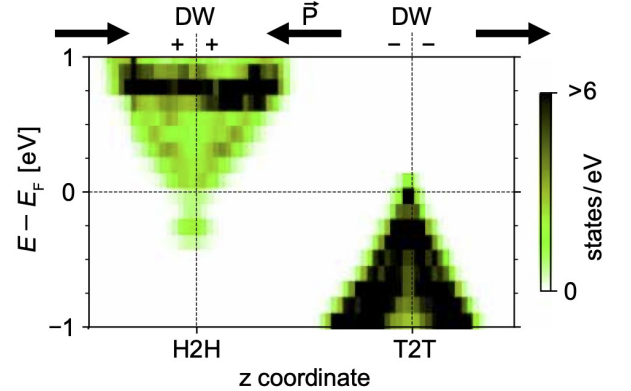


FIG. 4: Local density of states (DOS) of a super-cell when modelling a fully-charged H2H and a T2T DW in LN. The direction of polarization, the position of the Fermi energy, and the sign of the polarization charges are indicated. Note the very different DOS levels for the H2H and T2T DW.

In order to investigate the mechanisms behind the DWC, fully-charged head-to-head (H2H) and tail-to-tail (T2T) DWs of stoichiometric LN are modeled within DFT in the independent particle approximation (IPA). We thereby employ the VASP software package^{29,30}, PAW potentials implementing the PBE

formulation of the xc-functional^{31–33} and a cutoff energy for the plane wave basis at 500 eV. A H2H and a T2T DW are modelled within a $1 \times 1 \times 12$ repetition of the hexagonal unit cell and a $4 \times 4 \times 1$ k-point mesh. Thus, the two DWs, one H2H and one T2T, are separated by about 8 nm. Structural optimization reveals that the atomic positions and the local polarization reach the value of bulk LN at a distance of about 1–2 nm away from the DW center, which is in agreement with typical DW widths as deduced from TEM investigations³⁴. The local density of states of the super-cell for modelling the DW is shown in Fig. 4. The direction of polarization and the sign of the polarization charges are indicated as well. Interestingly, the spontaneous polarization causes a strong band bending for both types of fully-charged DWs, so that a non-vanishing portion of electronic states belonging to the conduction (valence) band, crosses the Fermi energy in proximity to the H2H (T2T) DW³⁵. The domain walls thus become semi-metallic, similar to suggestions in other materials^{18,19}. Moreover, the DOS at the H2H and T2T DW is very different; H2H DWs feature very low DOS values at the Fermi-energy and higher DOS values about 150 meV below it. Unfortunately, due to the limited precision of the DFT approach, it cannot be conclusively stated whether this gap in the H2H DWs DOS is related to the measured activation energy or not.

According to our calculations, a 2DEG is formed for fully-charged H2H and T2T DWs, that will contribute to the DWC. Nevertheless, a word of caution has to be expressed, addressing the interpretation of our DFT calculations in relation to the experiment:

- Firstly, improved methods beyond the IPA approach used here for calculating the electronic structure, are required to quantitatively estimate the overlap between conduction and valence bands.
- Second, non-charged or only slightly-inclined DWs, such as the DW measured in the present experiments, feature a less pronounced band bending and hence might not lead to the formation of a 2DEG. Whether the contribution of H2H and T2T walls within an oblique DW suffices to render the whole DW metallic is questionable.
- Third, the role of doping or defects, such as lithium vacancies or Mg-doping as used in the current experiment, is still unclear. They might easily lead to the formation of additional energy levels within the DWs (e.g., donor or acceptor levels) or shifts in the band structure.

Whether or not and to which extent different mechanisms such as the 2DEG formation, any polaron accumulation and charge hopping, etc. contribute to the DWC remains to be settled with further investigations. Nonetheless, this work demonstrates the feasibility to investigate DW band structures via first principle calculations and opens up the option of high DW currents.

In conclusion, our results consistently demonstrate that as temperature rises, there is a corresponding increase in the domain wall current (DWC). DWs, along with their conductivity,

remain stable even upon multiple heating cycles up to about 400°C, marking the highest temperatures documented in existing literature. This indicates the potential for developing DW-based electronics for high temperature-applications. At temperatures up to about 400°C, the thermally-activated nature of the DWC is confirmed, indicating that a hopping process (or similar mechanism) is also present for this temperature range. Here, no signs of saturation or an extrinsic conductivity region are found for the slightly-inclined DWs. Furthermore, DWs display varied activation energies in two overlapping temperature regimes, hinting towards the involvement of more than one type of defect/polaron to conduction, consistently observed within several DWs.

Acknowledgments

The authors gratefully acknowledge financial support by the Deutsche Forschungsgemeinschaft (DFG) through the Research unit FOR5044 (ID: 426703838; <https://www.for5044.de>). We thank Thomas Gemming and Dina Bieberstein for assistance in wafer dicing, as well as Henrik Beccard for assistance in sample preparation. EB and LME thank the Würzburg-Dresden Cluster of Excellence on “Complexity and Topology in Quantum Matter” - ct.qmat (EXC 2147; ID 39085490).

Data Availability Statement

The data that support the findings of this study are available from the corresponding author upon reasonable request.

- ¹G. Poberaj, H. Hu, W. Sohler, and P. Günter, “Lithium niobate on insulator (LNOI) for micro-phonic devices,” *Laser & Photonics Reviews* **6**, 488–503 (2012).
- ²R. Waser and A. Rüdiger, “Pushing towards the digital storage limit,” *Nature Materials* **3**, 81–82 (2004).
- ³D. Meier and S. Selbach, “Ferroelectric domain walls for nanotechnology,” *Nature Reviews Materials* **7**, 157–173 (2021).
- ⁴C. J. McCluskey, M. G. Colbear, J. P. V. McConville, S. J. McCartan, J. R. Maguire, M. Conroy, K. Moore, A. Harvey, F. Trier, U. Bangert, A. Gruvermann, M. Bibes, A. Kumar, R. G. P. McQuaid, and J. M. Gregg, “Ultrahigh Carrier Mobilities in Ferroelectric Domain Wall Corbino Cones at Room Temperature,” *Advanced Materials* **34**, 2204298 (2022).
- ⁵B. Kirbus, C. Godau, L. Wehmeier, H. Beccard, E. Beyreuther, A. Haußmann, and L. Eng, “Real-Time 3D Imaging of Nanoscale Ferroelectric Domain Wall Dynamics in Lithium Niobate Single Crystals under Electric Stimuli: Implications for Domain-Wall-Based Nanoelectronic Devices,” *ACS Applied Nano Materials* **2**, 5787 (2019).
- ⁶W. Geng, J. He, X. Qiao, L. Niu, C. Zhao, G. Xue, K. Bi, L. Mei, X. Wang, and X. Chou, “Conductive domain-wall temperature sensors of LiNbO₃ ferroelectric single-crystal thin films,” *IEEE Electron Device Letters* **42**, 1841 (2021).
- ⁷V. Y. Shur, A. R. Akhmatkhanov, and I. S. Baturin, “Micro- and nano-domain engineering in lithium niobate,” *Applied Physics Reviews* **2**, 040604 (2015).
- ⁸C. Werner, S. J. Herr, K. Buse, B. Sturman, E. Soergel, C. Razzaghi, and I. Breunig, “Large and accessible conductivity of charged domain walls in lithium niobate,” *Science Reports* **7**, 9862 (2017).
- ⁹C. Godau, T. Kämpfe, A. Thiessen, L. M. Eng, and A. Haußmann, “Enhancing the Domain Wall Conductivity in Lithium Niobate Single Crystals,” *ACS Nano* **11**, 4816–4824 (2017).
- ¹⁰Y. Zhang, Y. Qian, Y. Jiao, X. Wang, F. Gao, F. Bo, J. Xu, and G. Zhang, “Conductive domain walls in x-cut lithium niobate crystals,” *Journal Applied Physics* **132**, 044102 (2022).
- ¹¹W. Zhang, C. Wang, J. Lian, J. Jiang, and A.-Q. Jiang, “Erasable ferroelectric domain wall diodes,” *Chinese Physics Letters* **38**, 017701 (2021).
- ¹²P. Sharma and J. Seidel, “Neuromorphic functionality of ferroelectric domain walls,” *Neuromorphic Computing and Engineering* **3**, 022001 (2023).

- ¹³X. Chai, J. Lian, C. Wang, X. Hu, J. Sun, J. Jiang, and A. Jiang, "Conductions through head-to-head and tail-to-tail domain walls in LiNbO₃ nanodevices," *Journal of Alloys and Compounds* **873**, 159837 (2021).
- ¹⁴A. Suna, O. Baxter, J. McConville, A. Kumar, R. McQuaid, and J. M. Gregg, "Conducting ferroelectric domain walls emulating aspects of neurological behavior," *Applied Physics Letters* **121**, 222902 (2022).
- ¹⁵R. Turner, P. Fuierer, and R. Newnham, "Materials for high temperature acoustic and vibration sensors: A review," *Applied Acoustics* **41**, 299–324 (1994).
- ¹⁶M. Zahn, E. Beyreuther, I. Kiseleva, A. Lotfy, C. McCluskey, J. Maguire, A. Suna, M. Rüsing, J. Gregg, and L. Eng, "Equivalent-circuit model that quantitatively describes domain-wall conductivity in ferroelectric LiNbO₃," *Physical Review Applied* **21**, 024007 (2024).
- ¹⁷H. Beccard, E. Beyreuther, B. Kirbus, S. D. Seddon, M. Rüsing, and L. M. Eng, "Hall mobilities and sheet carrier densities in a single LiNbO₃ conductive ferroelectric domain wall," *Physical Review Applied* **20**, 064043 (2023).
- ¹⁸G. Nataf, M. Guennou, J. Gregg, D. Meier, J. Hlinka, E. K. H. Salje, and J. Kreisel, "Domain-wall engineering and topological defects in ferroelectric and ferroelastic materials," *Nature Reviews Physics* **2**, 634–648 (2020).
- ¹⁹P. S. Bednyakov, B. I. Sturman, T. Sluka, A. K. Tagantsev, and P. V. Yudin, "Physics and applications of charged domain walls," *npj Computational Materials* **4**, 65 (2018).
- ²⁰H. Beccard, B. Kirbus, E. Beyreuther, M. Rüsing, P. Bednyakov, J. Hlinka, and L. M. Eng, "Nanoscale Conductive Sheets in Ferroelectric BaTiO₃: Large Hall Electron Mobilities at Head-to-Head Domain Walls," *ACS Applied Nano Materials* **5**, 8717–8722 (2022).
- ²¹S. Y. Xiao, T. Kämpfe, Y. M. Jin, A. Haußmann, X. M. Lu, and L. M. Eng, "Dipole-Tunneling Model from Asymmetric Domain-Wall Conductivity in LiNbO₃ Single Crystals," *Physical Review Applied* **10**, 034002 (2018).
- ²²A. Haußmann, P. Milde, C. Erler, and L. Eng, "Ferroelectric Lithography: Bottom-up Assembly and Electrical Performance of a Single Metallic Nanowire," *Nano Letters* **9**, 763–768 (2009).
- ²³U. Yakhnevych, F. E. Azzouzi, F. Bernhardt, C. Kofahl, Y. Suhak, S. Sanna, K.-D. Becker, H. Schmidt, S. Ganschow, and H. Fritze, "Oxygen partial pressure and temperature dependent electrical conductivity of lithium-niobate-tantalate solid solutions," *Solid State Ionics* **407**, 116487 (2024).
- ²⁴C. Kofahl, L. Dörrer, H. Wulfmeier, H. Fritze, S. Ganschow, and H. Schmidt, "Hydrogen Diffusion in Li(Nb,Ta)O₃ Single Crystals Probed by Infrared Spectroscopy and Secondary Ion Mass Spectrometry," *Chemistry of Materials* **36**, 1639–1647 (2024).
- ²⁵E. Singh, H. Beccard, Z. H. Amber, J. Ratzemberger, C. W. Hicks, M. Rüsing, and L. M. Eng, "Tuning domain wall conductivity in bulk lithium niobate by uniaxial stress," *Physical Review B* **106**, 144103 (2022).
- ²⁶P. Reichenbach, T. Kämpfe, A. Haußmann, A. Thiessen, T. Woike, R. Steudtner, L. Kocsor, Z. Szaller, L. Kovács, and L. M. Eng, "Polaron-mediated luminescence in lithium niobate and lithium tantalate and its domain contrast," *Crystals* **8**, 214 (2018).
- ²⁷J. Koppitz, O. Schirmer, and A. Kuznetsov, "Thermal Dissociation of Bipolarons in Reduced Undoped LiNbO₃," *Europhysics Letters* **4**, 1055–1059 (1987).
- ²⁸O. Schirmer, M. Imlau, C. Merschjann, and B. Schoke, "Electron small polarons and bipolarons in LiNbO₃," *Journal of Physics: Condensed Matter* **21**, 123201 (2009).
- ²⁹G. Kresse and J. Furthmüller, "Efficient iterative schemes for ab initio total-energy calculations using a plane-wave basis set," *Physical Review B* **54**, 11169–11186 (1996).
- ³⁰G. Kresse and J. Furthmüller, "Efficiency of ab-initio total energy calculations for metals and semiconductors using a plane-wave basis set," *Computational Materials Science* **6**, 15–50 (1996).
- ³¹J. P. Perdew, K. Burke, and M. Ernzerhof, "Generalized gradient approximation made simple," *Physical Review Letters* **77**, 3865–3868 (1996).
- ³²J. P. Perdew, A. Ruzsinszky, G. I. Csonka, O. A. Vydrov, G. E. Scuseria, L. A. Constantin, X. Zhou, and K. Burke, "Restoring the density-gradient expansion for exchange in solids and surfaces," *Physical Review Letters* **100**, 136406 (2008).
- ³³P. E. Blöchl, "Projector augmented-wave method," *Physical Review B* **50**, 17953–17979 (1994).
- ³⁴J. Gonnissen, D. Batuk, G. F. Nataf, L. Jones, A. M. Abakumov, S. Van Aert, D. Schryvers, and E. K. H. Salje, "Direct Observation of Ferroelectric Domain Walls in LiNbO₃: Wall-Meanders, Kinks, and Local Electric Charges," *Advanced Functional Materials* **26**, 7599–7604 (2016).
- ³⁵L. M. Verhoff, M. Rüsing, L. Eng, and S. Sanna, "2D conductivity in insulating ferroelectrics: Peculiar properties of domain walls," in preparation.
- ³⁶M. Schröder, A. Haußmann, A. Thiessen, E. Soergel, T. Woike, and L. Eng, "Conducting Domain Walls in Lithium Niobate Single Crystals," *Advanced Functional Materials* **22**, 3936–3944 (2012).
- ³⁷I. Kiseleva, *Toward Reproducible Domain-Wall Conductance in Lithium Niobate Single Crystals*, Master's thesis, Technische Universität Dresden, Dresden, Germany (2023).
- ³⁸L. Ding, E. Beyreuther, B. Koppitz, K. Kempf, J. Ren, W. Chen, M. Rüsing, Y. Zheng, and L. M. Eng, "Comparative study of photo-induced electronic transport along ferroelectric domain walls in lithium niobate single crystals," (2024), arXiv:2402.17508 [physics.app-ph].